Molecular BioSystems

PAPER

View Article Online
View Journal | View Issue

Cite this: *Mol. BioSyst.*, 2015, 11, 1389

Elucidating the interaction of γ-hydroxymethyl-γ-butyrolactone substituents with model membranes and protein kinase C–C1 domains†

Rituparna Borah,‡ Narsimha Mamidi,‡ Subhankar Panda, Sukhamoy Gorai, Suraj Kumar Pathak and Debasis Manna*

Received 3rd February 2015,
Accepted 17th March 2015

DOI: 10.1039/c5mb00100e

www.rsc.org/molecularbiosystems

The protein kinase C (PKC) family of proteins is an attractive drug target. Dysregulation of PKC-dependent signalling pathways is related to several human diseases like cancer, immunological and other diseases. We approached the problem of altering PKC activities by developing C1 domain-based PKC ligands. In this report γ-hydroxymethyl-γ-butyrolactone (HGL) substituents were investigated in an effort to develop small molecule-based PKC regulators with higher specificity for C1 domain than the endogenous diacylglycerols (DAGs). Extensive analysis of membrane–ligands interaction measurements revealed that the membrane-active compounds strongly interact with the lipid bilayers and the hydrophilic parts of compounds localize at the bilayer/water interface. The pharmacophores like hydroxymethyl, carbonyl groups and acyl-chain length of the compounds are crucial for their interaction with the C1 domain proteins. The potent compounds showed more than 17-fold stronger binding affinity for the C1 domains than DAG under similar experimental conditions. Nonradioactive kinase assay confirmed that these potent compounds have similar or better PKC dependent phosphorylation capabilities than DAG under similar experimental conditions. Hence, our findings reveal that these HGL analogues represent an attractive group of structurally simple C1 domain ligands that can be further structurally altered to improve their potencies.

Introduction

The protein kinase C (PKC) family of proteins are involved in signal transduction and various cellular events including, apoptosis, proliferation, metabolism and others.[1,2] The PKC proteins contain a C-terminal catalytic domain and an N-terminal regulatory domain with an auto-inhibitory sequence, and one or two membrane targeting (C1 and C2) domains. Phosphorylation, increased concentration of diacylglycerol (DAG), and/or Ca^{2+} in the presence of anionic phospholipids activate these enzymes at the membrane surface and transmit their signals by phosphorylating specific proteins.[3,4] DAG binds to the C1 domains of both the classical (calcium-, DAG-, and phospholipid-dependent), and novel (calcium-independent, but DAG- and phospholipid-dependent) PKCs. The reversible cellular translocation of classical PKC isoenzymes to the plasma membrane is initially arbitrated by Ca^{2+} binding to the C2 domain, followed by DAG binding to the C1 domain. On the contrary, DAG binding to the C1 domain activates novel PKC isoenzymes. Membrane association results in a conformational change and allows PKC isoenzymes to penetrate further into the cellular membranes through DAG–C1 domain interactions. DAG binding results in folding-out of the N-terminal pseudo substrate sequence of the PKC enzyme from its catalytic site, which allows access of several substrates to the catalytic site of the PKC enzymes.[5–9]

PKC isoenzymes play a pivotal role in the pathology of several diseases including cancer and Alzheimer's diseases.[10,11] Therefore, PKC isoenzymes have been a subject of intensive research and drug development. On the other hand, the catalytic domain of PKC enzymes is highly homologous with several other protein kinases in human genome. Hence, regulation of PKC enzyme activity by targeting its C1 domain provides a more conventional approach. Several studies have already shown that the regulatory domain of PKC isoenzymes might have independent biological functions.[2,9,12–16] The C1 domains are smaller in size (~50 residues), retain conserved structure, and contain only one ligand binding domain. In addition, the number of proteins containing this

Department of Chemistry, Indian Institute of Technology Guwahati, Assam 781039, India. E-mail: dmanna@iitg.ernet.in; Fax: +91 03 61258 2350; Tel: +91 03 61258 2325

† Electronic supplementary information (ESI) available: Characterization data of the synthesized compounds. Copies of ^{1}H and ^{13}C NMR spectra of the compounds. Molecular docking results of the compounds. Monomeric binding assay and FRET-based competitive binding assay of the compounds. See DOI: 10.1039/c5mb00100e

‡ R.B. and N.M. contributed equally to this work.

C1 domain is small. In consequence, a variety of PKC regulators directed to the C1 domain have been developed as a new class of antitumor agents.[4,17,18] C1 domain ligands such as bryostatin-1 are in clinical trials and ingenol-3-angelate is in clinical use.[19,20] Phorbol esters, which strongly bind with the C1 domains, have provided pharmacological tools for studying PKC function and activity. However, phorbol esters are known to promote tumors.[19–21] Compounds like prostratin, gnidimacrin, and DPP (12-deoxyphorbol-13-phenylacetate) have also shown PKC enzyme dependent antitumor activities in mice and selected human cell lines.[10,22]

Phorbol esters, bryostatin and other reported high-affinity C1 domain binding ligands are structurally complex, and they bind competitively to the DAG-binding site of the C1 domain with affinities several orders of magnitude higher than only DAGs.[23,24] The conformationally rigid scaffold of these C1 domain ligands made it difficult to alter their specificity and large-scale production. However, conformationally restricted DAG-lactones are reported to have intermediate potency between DAG and phorbol esters.[21–24] It is also deduced that the structural rigidity of DAG-lactones reduce the number of possible rotameric forms of DAGs, and one of the rigid rotamers mimics the actual conformation of physiologically active DAGs. The stronger binding of a DAG-lactone to a PKC–C1 domain than only DAG apparently is governed by a smaller decrease in entropy. Stronger binding is also governed by the presence of required pharmacophores and proper orientation of the ligands inside the binding pocket and their localization at the membrane bilayer. Structural and functional studies of the PKC–C1 domains have revealed that Thr-12, Leu-21, and Gly-23 residues play a crucial role in ligand binding. The hydrophobic residues present along the circumference of the binding pocket interact with the hydrophobic moiety of the ligand and facilitate insertion of the C1 domain into the membrane after ligand binding, thereby stabilizing the formation of the ternary (ligand–receptor–membrane) binding complex. In an attempt to develop C1 domain ligands that are simple and readily amenable to the introduction of a structural variation template, we used (*S*)-γ-hydroxymethyl-γ-butyrolactone (HGL). The other objective of designing these simple molecules is to overcome the spread in potency between complex natural product ligands and DAG.

The present study describes the design, synthesis, aggregation behaviour in aqueous solution, interaction with liposomes, *in vitro* binding properties of HGL substituents to the C1b subdomain of PKCδ and PKCθ, and their PKC enzyme activity. The results demonstrate that the C1 domain binding potencies of these compounds correlates well with their effect on membrane fluidity and hydration. The potent HGL analogues bind competitively to the DAG-binding site of the C1 domains of PKC. The γ-hydroxymethyl group, carbonyl groups of lactone, and ester of the active compounds play a crucial role in PKC–C1 domain binding. At lower micromolar concentrations, these HGL analogs also activate PKC enzyme. Overall, the results expand our understanding on the molecular parameters affecting PKC–C1 domain binding to membranes by synthetic HGL analogues.

Results and discussion

Design and synthesis

Structure–activity relationship (SAR) studies showed that hydroxymethyl and carbonyl functional groups of DAGs, DAG-lactones and phorbol esters play an important role for their interactions with the backbone amide protons and carbonyl of PKC–C1 domains. However, all these ligands have differential C1 domain binding potencies. Conformationally rigid phorbol esters have more than 1000-fold stronger binding affinity for a C1 domain than structurally simple and flexible DAGs. Several conformationally-constrained DAG-lactones showed intermediate C1 domain binding potency.[25–27] Inspired by the structural rigidity and higher binding affinity of the DAG-lactones, we selected (*S*)-γ-hydroxymethyl-γ-butyrolactone (HGL) analogues for the devolvement of PKC–C1 domain modulators. The HGL moiety provides a rigid five-membered ring as in DAG-lactones, but the HGL analogues are structurally different due to the position of its ester linkage and number of hydrophobic 'tails' (Fig. 1).

These compounds also retain necessary pharmacophores, namely hydroxyl and carbonyl functionalities within the same molecule, and hydrophobic tails important for membrane interaction (Fig. 1). Unlike most of the potent C1 domain ligands like phorbol esters, bryostatins and others, HGLs are structurally simpler and contain lesser rigidity. Structural modifications and large sale productions of HGLs are comparatively easier than those from potent natural products.[25–27] The HGLs (**1–3**) were synthesized in five to six steps from the L-glutamic acid as a starting material. HGLs with long (palmitic acid) and short chain (octanoic acid and propanoic acid) acids were synthesized in order to study the impact of hydrophobicity on the binding affinity. The synthesis was accomplished *via* a modified reported reaction protocol.[28] We initially prepared HGL analogous **1a** and **1b** in order to investigate the role of hydroxymethyl and hydroxyl groups on the binding of C1b subdomains of PKC isoforms. Compounds **1a** and **1b** were prepared in five steps from L-glutamic acid. The (*S*)-γ-hydroxymethyl-γ-butyrolactone (**5**) was synthesized from L-glutamic acid in two steps according previously reported procedures and the hydroxyl group was protected with

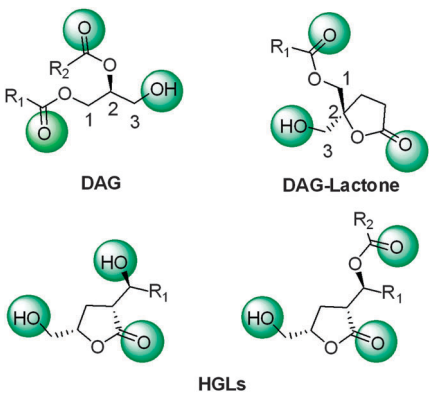

Fig. 1 Structures of DAG, DAG-lactones and γ-hydroxymethyl-γ-butyrolactone (HGLs) indicating the crucial pharmacophores required for PKC–C1 domain binding.

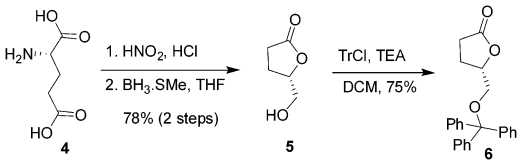

Scheme 1 Synthesis of protected γ-butyrolactone (**6**).

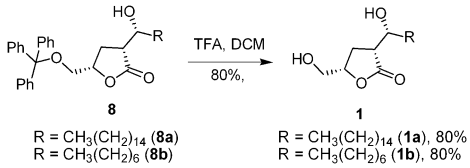

Scheme 2 Synthesis of α-hydroxylmethyl-γ-lactone derivative (**1**).

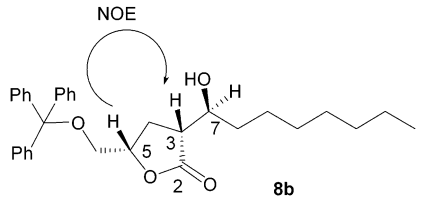

Fig. 2 Stereochemical assignments of product **8b** based on COSY and NOE experiment.

tritylchloride in the presence of triethyl amine in good yield (Scheme 1).[28]

After that, the model aldol-reaction was conducted between the protected γ-butyrolactone (**6**) and octanal (**7b**) in the presence of various bases such as NaH, triethyl ammonia (TEA), DIPEA, DBU and DABCO; but even after 24 h we did not obtain the desired product. In order to screen the bases/optimize the reaction conditions, we performed the same reaction with LDA (1.5 equiv.) in the presence of CuCN/LiCl (1.0 equiv.)/(2.0 equiv.) as an additive at −78 °C and obtained the desired aldol adduct **8b** in 70% isolated yield (Table S1, ESI,† entry 6) whereas in case of *n*-BuLi (1.5 equiv.) the yields were increased up to 80% (Table S1, ESI,† entry 7) in presence of the same additive ratio. We used several other Lewis acids as an additive to improve the yields of the products; unfortunately no fruitful result was obtained. Therefore, *n*-BuLi (1.5 equiv.) and CuCN/LiCl (1.0 equiv./2.0 equiv.) as an additive in dry THF solvent (at −78 °C), was chosen as the best reaction condition (with 80% yield within 20 min) for the aldol reaction. The reaction generated only one diastereomer (**8b**) with (*S*, *R*, *S*) configurations, which was confirmed by cosy and NOE experiments (Fig. 2). There was a strong interaction between the C3 and C5 protons in the COSY experiment. This reveals that these two protons are on the same plane. The coupling constant of C3 proton and C7 proton, $J = 7.7$ Hz, indicates that these two protons are *trans* to each other.[28] The reaction was also performed with two more aldehydes under this optimized reaction condition and the results are summarized in Table 1. The synthesis of dialcohol **1a** and **1b** (in 80% yield) was accomplished *via* careful removal of the trityl group under trifluoroacetic acid conditions as shown in the Scheme 2. To verify the hydrophobicity effect of the ligands on the biding affinity, we also prepared HGL ester derivatives by introducing a long chain fatty acid (palmitic acid) and short chain acids (octanoic acid, propanoic acid). The acyl chains were then introduced into alcohol **10** using a standard *N*,*N*′-dicyclohexylcarbodiimide (DCC)-mediated coupling reaction with readily available carboxylic acids (palmitic acid/caprylic acid/propanoic acid) to produce compounds **2** and **3** in good yield as shown in Table 2. Finally, the trityl group was de-protected under trifluoroacetic acid conditions to access HGL derivatives in good yield.

Table 1 Aldol reactions[a]

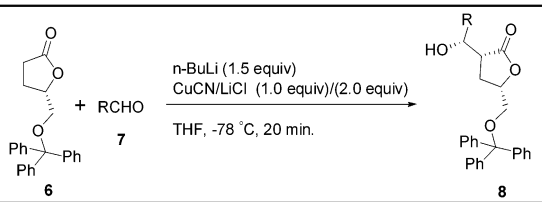

Aldehyde	Product	Yield[b] (%)
$CH_3(CH_2)_{14}CHO$ (**7a**)	**8a**	80
$CH_3(CH_2)_6CHO$ (**7b**)	**8b**	80
CH_3CH_2CHO (**7c**)	**8c**	85

[a] Performed with protected γ-lactone (1.0 equiv.), *n*-buLi (1.5 equiv.), CuCN/LiCl (1.0 equiv.)/(2.0 equiv.) and aldehyde (1.5 equiv.) in dry THF. [b] Isolated yields.

Aggregation studies of the compounds

To check the behaviour of the compounds in aqueous solution, we first investigated their aggregation behaviours by measuring the fluorescence properties of a polarity indicator, pyrene. Concentration-dependent aggregation behaviours of the compounds and simultaneous inclusion of pyrene molecules into hydrophobic cores of the aggregates was reflected by an increase in pyrene fluorescence intensity. The fluorescence intensity ratio, I_1/I_3 of pyrene was considered as a measure of the polarity of its microenvironment and was further used to calculate critical aggregation concentration (CAC) values of the compounds (Fig. S8, ESI†).[29] The measured CAC values of the compounds **1a**, **2a**, and **3a** were 60, 22, and 43 μM, respectively (Fig. 3). Above the CAC values, the higher and lower ratios of I_1/I_3 indicate the polar (loose aggregates) and hydrophobic (compact aggregates) environments. These results show that, above 50–70 μM compound concentrations, the ratio of I_1/I_3 reached a plateau region. However, with further increase in concentrations the I_1/I_3 ratio gradually reduced, signifying the formation of loosely bound aggregates in aqueous solution with an extensive concentration range. The results also indicate that tested compounds aggregate at lower concentration ranges in aqueous solution, possibly due to the absence of charge head groups. Investigation of these CAC ranges of aggregate formation is essential in understanding their interaction properties both with the lipid bilayers and PKC–C1 domain under monomeric form in aqueous solution.

Table 2 Synthesis of γ-butyrolactone derivatives

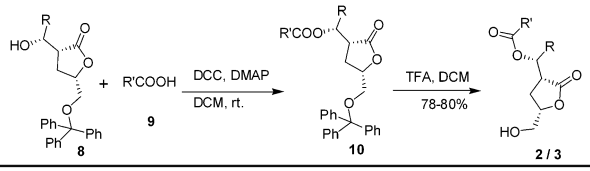

Compound	R	R′	Compound	R	R′
10ac	$CH_3(CH_2)_{14}$ (**8a**)	CH_3CH_2 (**9c**)	**2a**	$CH_3(CH_2)_{14}$	CH_3CH_2
10ab	$CH_3(CH_2)_{14}$ (**8a**)	$CH_3(CH_2)_6$ (**9b**)	**3a**	$CH_3(CH_2)_{14}$	$CH_3(CH_2)_6$
10bc	$CH_3(CH_2)_6$ (**8b**)	CH_3CH_2 (**9c**)	**2b**	$CH_3(CH_2)_6$	CH_3CH_2
10ba	$CH_3(CH_2)_6$ (**8b**)	$CH_3(CH_2)_{14}$ (**9a**)	**3b**	$CH_3(CH_2)_6$	$CH_3(CH_2)_{14}$

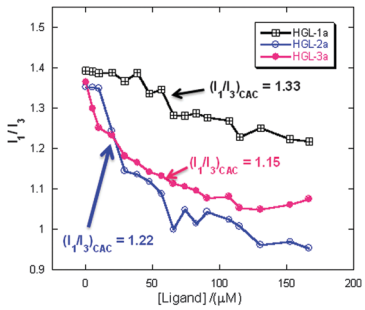

Fig. 3 Measurement of critical aggregation concentration of compounds **1a**, **2a**, and **3a** in aqueous solution. Plot of pyrene fluorescence intensity ratio I_1/I_3 against increasing concentration of compounds. [Pyrene] = 2 μM, λ_{ex} = 380 nm.

Membrane–ligand interaction measurements: orientation of ligands at the interface

Surface pressure (π)–area (*A*) isotherms provide an insight into how chemical structure and physical behaviour, including intramolecular and intermolecular interactions, modify the assembly of the amphiphilic molecules at the air/water interface.[30,31] The π–*A* isotherms of the pure compounds displayed a slightly different assembly pattern from compounds in the presence of DPPC lipid (Fig. 4). However, the assembly properties of the pure compounds **2a** and -**3a** are significantly different from pure DPPC lipids under similar experimental conditions. The isotherms also indicate that these compounds become partly soluble with an increase in lateral pressure. The π–*A* isotherms of these pure compounds show a profound liquid-expanded (LE) phase and a subsequent LE–liquid condensed (LC) region and a more condensed phase during the compression process. The LE phase of these pure compounds, and compounds in the presence of DPPC lipid, begin at a much higher molecular area of 250 Å^2 indicating a very loose configuration of the molecules within the fluid monolayer. The presence of LE–LC is indicated by the plateau region in the isotherm. The additional ordering in π–*A* isotherms and significant change in the LE–LC region of these compounds in the presence of DPPC lipid may be due to their interaction properties between their head groups and hydrophobic 'tails' (Fig. 4). It is also important to note that the presence of acyl groups demonstrate significant effects on the monolayer properties of the compounds; however, alternative hydrophobic groups show almost no effect on the monolayer properties of the compounds. Nevertheless, monolayer properties of the compounds in the presence of DPPC lipid clearly depict their strength of interaction. Therefore, the hydroxyl-lactone moiety of the compounds strongly affects the assembly properties and its interactions with the DPPC molecules, and also lipid interactions play a significant role in the monolayer organization of the molecules.

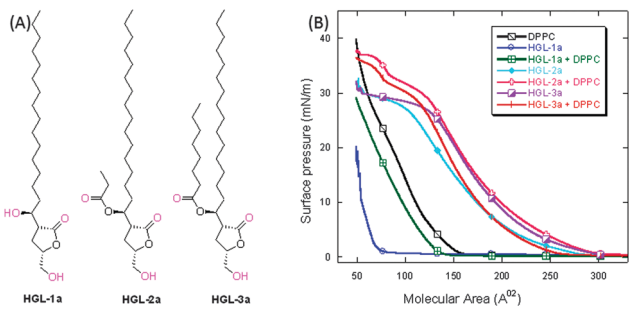

Fig. 4 Structure of the membrane active compounds (A). Surface pressure (π)–molecular area (*A*) isotherm of the saturated hybrid lipids (B).

Measurement of change in fluidity and hydration of the lipid bilayer

To recognize the consequences of membrane active compounds upon the fluidity of the lipid bilayer and dynamics of lipid molecules, we measured the fluorescence anisotropy of the membrane active 1,6-phenyl-1,3,5-hexatriene (DPH) molecules under liposomal environment. The hydrophobic DPH molecules are known to embed within the hydrophobic core of the lipid bilayers, allowing estimating the modulation of lipid-bilayer fluidity induced by membrane-active compounds.[29] Fig. 5A represents the anisotropy values of DPH molecules in the presence/absence of the compounds under liposomal environment. The anisotropy value of DPH in the presence of compound **2a** is slightly smaller than with the other compounds, indicating increase in bilayer fluidity. Changes in membrane surface were monitored by a dansyl-PE probe. The fluorescence signal of dansyl is environmentally sensitive and efficiently gets quenched by water.[32,33] The increase in % mole of membrane active HGL compounds induces an increase in dansyl fluorescence quenching (Fig. 5B). The increase in quenching can be correlated with the increase in dansyl-PE head group hydrations at the membrane surface, which correlates well with the increase in membrane fluidity in the presence of these compounds.

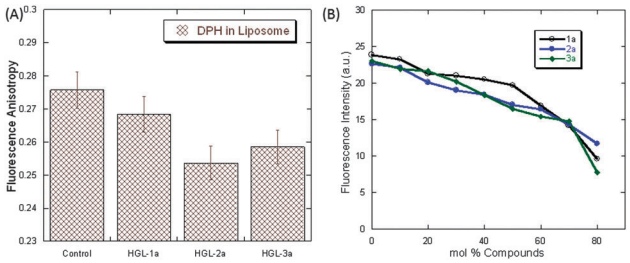

Fig. 5 Membrane fluidity and hydration change measurements. Fluorescence anisotropy of DPH embedded in PC/cholesterol/ligand (60/20/20) liposomes. Control: no ligand was added to the liposomes (A). Effect of compounds on the fluoresce intensity of dansyl-PE embedded in PC/cholesterol/dansyl-PE (79/20/1) liposomes (B). Values represent the mean ± SD from triplicate measurements.

Extent of membrane localization

The structural analysis reveals that the head groups of DAG and HGLs are anticipated to be placed near the bilayer/water interfacial region. However, the extent of localization of these pharmacophores containing head groups at the bilayer/water interface is crucial for their capability to interact with the C1 domains. For this reason we determined sodium dithionite-induced fluorescence quenching rates of the NBD moiety using DPPC/ligand/NBD-PE liposomes. The NBD moiety of NBD-PE lipid is reported to be embedded close to the bilayer interface, providing a useful marker for surface interactions of membrane-active C1 domain ligands.[34–36] The measured NBD fluorescence quenching rates propose that the NBD moiety became more ''shielded'' from the soluble dithionite quencher because of the presence of ligands within the liposomes (Fig. 6). Therefore, membrane environment modification by these compounds may enhance the ability of a C1 domain to insert into the membrane. The results also suggest that these compounds are more localized at the bilayer/water interface and more accessible for protein binding than DAG_{16}.

Protein–ligand interaction measurements

In the present study, the C1b subdomains of PKCδ, PKCθ isoenzymes were used to measure the binding parameters of HGLs. These C1b subdomains have sufficiently strong DAG binding affinities and are easy to purify from bacterial cells. The binding-potencies of the compounds were measured by a Trp-fluorescence quenching method, steady-state fluorescence anisotropy, and Förster resonance energy transfer (FRET)-based competitive binding assay.

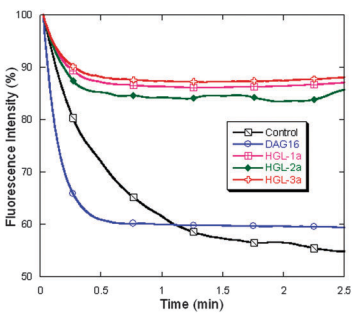

Fig. 6 Fluorescence quenching of NBD-PE embedded in PC/$ligand_{16}$/NBD-PE (89 : 10 : 1) liposomes. Sodium dithionite = 0.6 μM. Control: no ligand.

Interaction with soluble ligands

Trp-fluorescence properties of the proteins are widely used to examine the ligand-induced changes in protein conformation and/or microenvironment. The presence of a single Trp-residue (Trp-252 in delta, Trp-253 in theta) close to the ligand binding site makes these C1b subdomains a model system to monitor ligand binding properties. The ligand-induced Trp-fluorescence quenching data in the native state (insignificant or no shifting in emission peak position observed) was used to determine the binding affinity of the C1b subdomains for the ligands in monomeric form. The compound concentrations used during the spectroscopic measurements were well below their CAC values, indicating their monomeric form under the experimental conditions. The ligand binding can cause an environmental change for Trp-residue, exposing it to a hydrophilic environment. This could lead to a decrease in the Trp-emission signal with increasing concentrations of the compounds (Fig. 7 and Fig. S9, ESI†). The calculated binding parameters revealed that compounds **2** and **3**, with different chain lengths, strongly interact with the C1b subdomains. In particular, monomeric ligands **2b** and **3b** show more than 9- and 15-fold stronger binding affinity than DAG_8 for PKCδ–C1b subdomain (Table 3). To understand the importance of hydrophobicity of the compounds in protein binding, a similar analysis was performed with the long-chain HGL derivatives. Although there is a distinct difference in hydrophobicity between compounds like **3a** and **3b**, they show only a subtle difference in their protein binding affinities. This could be due to their binding orientations with the C1b subdomains. The binding of these compounds with the C1b subdomains is mostly governed by hydrogen bonding with the amino acid backbone through their γ-hydroxymethyl and carbonyl functionalities. In addition, hydrophobic interaction among the compounds and amino acid residues at the circumference of the binding pocket may play an important role in

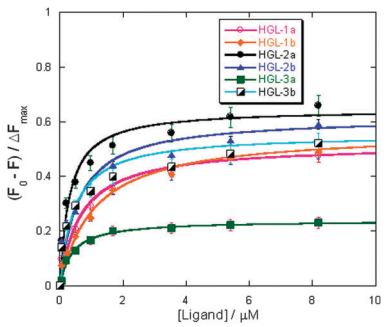

Fig. 7 Binding of compounds with the PKCδ–C1b subdomain. Representative plot of Trp-fluorescence intensity of PKCδ–C1b (1 μM) in buffer (20 mM Tris, 160 mM NaCl, 50 μM $ZnSO_4$, pH 7.4) in the presence of varying concentration of **1–3**, where F and F_0 are fluorescence intensity in the presence and absence of the ligands, respectively. The solid lines are nonlinear least-squares best-fit curves. Values represent the mean ± SD from triplicate measurements.

Table 3 Ligand binding parameters of PKCδ C1b and PKCθ C1b proteins[a] at room temperature

	K_D(ML)/(μM)			K_D(ML)/(μM)	
Compound	PKCδ C1b	PKCθ C1b	Compound	PKCδ C1b	PKCθ C1b
DAG_{16}	6.57 ± 0.23	7.14 ± 0.39	DAG_8	11.37 ± 0.69	6.92 ± 0.39
1a	0.89 ± 0.11	0.81 ± 0.12	**1b**	1.33 ± 0.12	0.68 ± 0.11
2a	0.40 ± 0.14	0.33 ± 0.08	**2b**	1.02 ± 0.15	0.30 ± 0.09
3a	0.38 ± 0.09	0.98 ± 0.09	**3b**	0.73 ± 0.19	1.19 ± 0.19

[a] Protein, 0.25 μM in buffer (20 mM Tris, 160 mM NaCl, 50 μM $ZnSO_4$, pH 7.4). Values represent the mean ± SD from triplicate measurements.

ligand binding affinities of the protein. The long alkyl chains facilitate the compounds to interact with the membrane bilayer, where PKC proteins interact with the membrane through the C1 domain for activation and regulation of various cellular pathways. A similar trend in binding affinities was also observed with the reported C1 domain ligands. However, these binding parameters of the compounds in monomeric form do not show a clear specificity for either PKCθ or PKCδ–C1 domains.

Molecular docking analysis

In order to better understand the possible binding mode of the compounds and the interacting residues of the proteins, we performed molecular docking analysis using the crystal coordinates of the PKCδ–C1b in complex with phorbol-13-*O*-acetate (1PTR).[37] The molecular models revealed that the HGLs were anchored to the binding site in a similar fashion as phorbol esters and DAG-lactones.[26] The most effective compound, **2b**, showed three possible hydrogen bonds with the amino acid backbone. The hydroxymethyl group was hydrogen bonded to the carbonyls of L251. The carbonyl group of the lactone moiety formed a hydrogen bond with the backbone amide proton of G253. An additional hydrogen bonding was also observed between side chain amine of Q257 with the carbonyl group of ester moiety. A similar hydrogen bonding network was also observed between compound **3b** and the PKCδ–C1b protein. Whereas, the hydroxyl group of compound **1b** showed five hydrogen bondings with the backbone amide proton and carbonyls of T242 and L251 and the side chain amide proton of Q257 (Fig. 8). However, the binding affinity measurements and molecular docking analysis do not corroborate. This could be due to the strength of interaction and the conformational adjustments of the protein and compounds under experimental conditions and also the contribution of bridging water molecules between HGLs and C1 domains could generate stronger interactions.

Steady-state anisotropy measurements

We also performed steady-state fluorescence anisotropy measurements of the proteins in absence or presence of the ligands to gain more information of the ligand–protein interaction. The degree of anisotropy of pure PKCδ C1b protein increases from 0.0439 in buffer to 0.0874 and 0.0850 on interactions with 10-fold excess of ligands **2b** and **3b**, respectively (Table S2, ESI†). Similar increases in anisotropy values were also observed for proteins in presence of DAGs and other compounds. Although the increases in anisotropy values were different for the compounds, this experiment still suggests that the presence of compounds increase the rigidity of the surrounding environment of the protein.

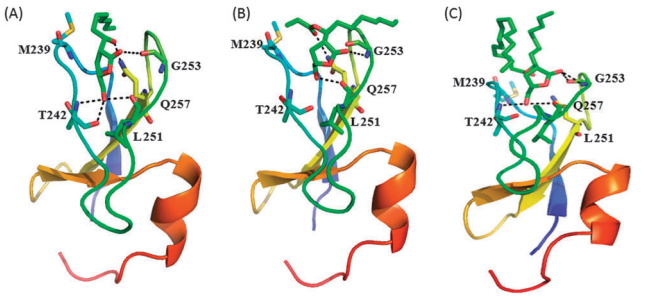

Fig. 8 Structures of ligand-bound PKCδ–C1b subdomains. Modelled structure of **1b** (A), **2b** (B) and **3b** (C) docked into PKCδ–C1b (1PTR) subdomain. The modelled structures were generated using the Molegro Virtual Docker, version 4.3.0. The oxygen atoms and nitrogen atoms are shown in red and blue, respectively. The dotted line (black) indicates possible hydrogen bonds.

Interaction with ligand associated liposomes

The PKC–C1 domains contain a membrane binding groove along with its DAG-binding site. Under physiological conditions DAG-dependent membrane binding and/or penetration of the C1 domain in the presence of anionic phospholipids activates PKC isoenzymes and regulates its cellular activities. Consequently, C1 domain binding properties of the compounds were measured under membrane environment using protein to membrane FRET-based competitive binding assay. Trp-residue of the C1b subdomains acts as the FRET donor and a low density of membrane-inserted dansyl-PE (dPE) lipid provides the acceptor. DAG_8 was used as a competitive inhibitor for this assay. Anionic phospholipids, in particular phosphatidylserine, is known to induce the DAG-dependent membrane binding of the C1 domain through its interaction with the cationic groove.[12,26,34,38] Hence, PS was incorporated into the liposomes. Additional zwitterionic lipid PE was used to form stable liposomes. The reduction in the protein-to-membrane FRET signal (Fig. S10, ESI†) was inspected to determine the competitive displacement of C1b subdomains from the liposomal surface to the bulk solution and apparent inhibitory constant [$K_I(DAG_8)_{app}$] calculation (Fig. 9 and Fig. S11, ESI†). The measurements were performed for membrane active compounds **1a**, **2a** and **3a**. The binding parameters demonstrated that compound **2a** has stronger binding affinity for the PKCθ–C1b subdomain than the other compounds under the liposomal

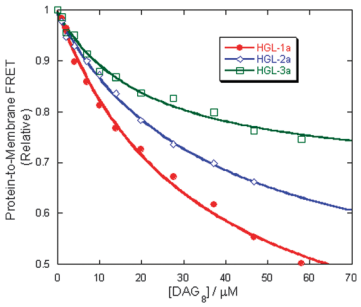

Fig. 9 Competitive displacement assay for the PKCδ–C1b subdomains (1 μM) bound to liposome containing ligands **1a**, **2a** and **3a**. The bound complex was titrated with the DAG_8.

Table 4 Equilibrium binding parameters for PKCδ C1b and PKCθ C1b protein[a] with the ligand-associated liposomes[b] at room temperature

	$K_I(DAG_8)_{app}$/(μM)		$K_D(L_{16})$/(nM)	
Compound	PKCδ C1b	PKCθ C1b	PKCδ C1b	PKCθ C1b
1a	33.39 ± 1.95	34.12 ± 1.19	72.02 ± 5.91	63.95 ± 5.12
2a	36.95 ± 2.01	51.75 ± 3.74	28.78 ± 7.89	16.88 ± 1.95
3a	22.19 ± 1.68	25.90 ± 2.57	45.82 ± 7.01	103.43 ± 6.98

[a] Protein, 1 μM in buffer (20 mM Tris, 150 mM NaCl, 50 μM $ZnSO_4$, pH 7.4). [b] Active liposome composition, PC/PE/PS/dPE/ligand (55/15/20/5/5). Values represent the mean ± SD from triplicate measurements.

environment. This competitive displacement assay also verifies that the potent compounds preferably interact with the C1b subdomains through its DAG/phorbol ester binding site. We have also calculated the equilibrium dissociation constant (K_D(L)) for the C1b subdomains binding to the liposome-associated targeted ligand using eqn (4). Comparison of the equilibrium dissociation constant also revealed that C1b subdomains have higher binding affinity for the compound **2a** associated liposomes (Table 4). Therefore, the *in vitro* C1 domain binding measurements pointed out that higher concentration of DAG_8 was required for the displacement of C1b subdomains from the compound **2a**-associated liposomes. Direct protein binding to the compound containing liposomes also showed strong binding affinities (Table S3, ESI†).

PKC activity assay

To verify the feasibility of the synthesized HGL compounds in activating PKC enzymes, PepTag-nonradioactive kinase activity assay was performed in the presence of PS.[39,40] In this assay PKC enzyme-specific florescent peptide was used as substrate. PKC-dependent phosphorylation of the fluorescent peptide changes the net charge from +1 to −1, allowing the phosphorylated and non-phosphorylated florescent peptide to be separated by an agarose gel electrophoresis method. The phosphorylated fluorescent peptide migrated toward the positive electrode and a relative amount of phosphorylated fluorescent peptide was further quantified by fluorescence spectral analysis according to the manufacturer's protocols. The results showed that under the similar experimental condition the potent compounds have similar or better PKC activating capabilities than DAG (Fig. 10 and Fig. S12, ESI†). In contrast to our C1 domain binding affinities for both monomeric form and under liposomal environment,

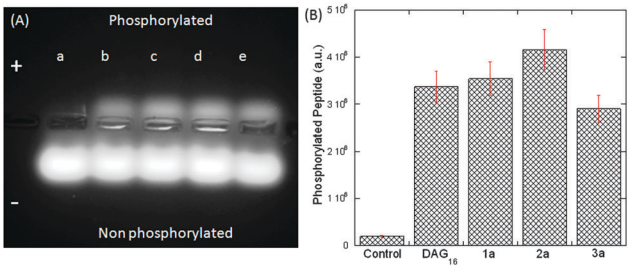

Fig. 10 The PKC activity in the absence and presence of DAG_{16} and potent compounds (8 μM). Representative UV-illuminated agarose gel image of the product of reactions run with PKC full-length enzyme. Control with no PS containing PKC activator solution and activator (lane a). Activity assay in the presence of DAG_{16} (lane b) and potent compounds **1a** (lane c), **2a** (lane d) and **3a** (lane e) (A). Relative amounts of phosphorylated PepTag C1 peptide were calculated from fluorescence spectral analysis (B).

PKC activity assay did not show any significant differences in their phosphorylation capabilities among the potent compounds. Therefore, further studies are required to resolve their potency differences. However, the activity assay confirms that the synthesized potent HGL compounds activate PKC enzyme under the experimental conditions.

These studies show that the membrane active HGL derivatives interact with phospholipids and influence their monolayer/bilayer properties. The pharmacophores-containing moiety, γ-hydroxymethyl-γ-butyrolactone of the compounds is preferably localized at the water/bilayer interface and accessible for PKC–C1 domain binding. The binding parameters and molecular docking analysis of the compounds highlight the importance of pharmacophores, hydrophobicity, and binding orientations of the ligands. The binding properties also suggest that membrane active compounds can differentially influence the *in vitro* membrane interaction properties of the C1 domains of PKCδ and PKCθ enzymes. The compound **2a** has a little stronger binding affinity for both the C1 domains than other compounds. We hypothesize that this modest stronger binding affinities of compound **2a** could be because of the presence of a propionate group along with a membrane-active hydrophobic 'tail', which allow the compound to interact strongly with hydrophobic residues surrounding the ligand binding site of the C1 domains or the effect of compound **2a** on the lipid bilayer organization. We also presume that the presence of these compounds makes the bilayer structure more loosely packed, allowing the C1 domains to bind with the HGLs and penetrate into the lipid bilayer, which is critical for the PKC enzyme activation at the inner-plasma membrane surface. However, the negligible binding potency difference between PKCδ- and PKCθ–C1b domains could be because of the dissimilarities in surface areas and the residues present within the binding site. Our nonradioactive kinase activity assay clearly showed that HGLs activate the PKC enzymes in a similar manner as that of DAG. PKC activating capabilities of these compounds could be lower than a phorbol ester or other structurally complex molecules under similar experimental conditions; however, we successfully developed structurally restricted γ-butyrolactone-based simple C1 domain ligands.

Conclusion

In this study we demonstrated that γ-hydroxymethyl-γ-butyrolactone substituents strongly interact with the model membrane and C1 domain of novel PKC isoenzymes. Strong interaction between compounds and the model membrane alter its monolayer/bilayer properties including fluidity and hydration. The protein binding properties suggest that hydroxymethyl and acyl-groups of the compounds are important for C1 domain binding through its DAG/phorbol ester binding site. The enhanced fluidity of the lipid bilayer structures could allow the PKC–C1 domains to interact strongly with the HGL derivatives in the presence of anionic phospholipids. Protein kinase activity assay also confirmed that these potent compounds can activate PKC enzymes. Therefore, our findings suggest that these hydroxymethyl γ-butyrolactone substituents are potential regulators of PKC isoforms and can be used in PKC-based drug development processes.

Experimental section

General information

All chemicals were purchased from Sigma (St. Louis MO), SRL (Mumbai, India) and used for synthesis without further purification. Dry solvents were obtained as per reported procedures. Reactions were performed under nitrogen atmosphere and monitored using thin layer chromatographic (TLC) plates prepared from silica gel 60 F254 (0.25 mm). Compounds were purified through column chromatography using 60–120 mesh silica gel. NMR spectra were recorded using $CDCl_3$ (δ = 7.24 for ^{1}H and δ = 77.23 for ^{13}C NMR) with Varian 400 MHz and Bruker 600 MHz spectrometers. Coupling constants (J values) are reported in hertz, and chemical shifts are reported in parts per million (ppm) downfield from tetramethylsilane using residual chloroform (δ = 7.24 for ^{1}H NMR, δ = 77.23 for ^{13}C NMR) as an internal standard. Multiplicities are reported as follows: s (singlet), d (doublet), t (triplet), m (multiplet), and br (broadened). Mass spectra were recorded using a Waters Q-TOF Premier mass spectrometer system, and data were analysed using the built-in software. 1,2-Dipalmitoyl-*sn*-glycerol (DAG_{16}), 1,2-dioctanoyl-*sn*-glycerol (DAG_8), 1,2-dipalmitoyl-*sn-glycero*-3-phosphocholine (DPPC), 1,2-dipalmitoyl-*sn-glycero*-3-phospho-L-serine (DPPS), 1,2-dipalmitoyl-*sn-glycero*-3-phosphoethanolamine (DPPE), 1,2-dioleoyl-*sn-glycero*-3-phosphoethanolamine-*N*-(5-dimethylamino-1-naphthalenesulfonyl) (NBD-PE) and *N*-[5-(dimethylamino)naphthalene-1-sulfonyl]-1,2-dihexadecanoyl-*sn-glycero*-phosphoethanol -amine (Dansyl-PE) were purchased from Avanti Polar Lipids (Alabaster, AL). The PepTag-nonradioactive kinase activity assay kit was obtained from Promega (Madison, WI). Ultrapure water (Milli-Q system, Millipore, Billerica, MA) was used for the preparation of buffers.

General procedure for the synthesis of γ-butyrolactone carboxylic acid

To a stirring solution of L-glutamic acid (1.0 equiv.) in water was added HNO_2 (1.2 equiv.) followed by HCl (1.2 equiv.) at 0 °C and stirring was continued for 8 h. After completion of the reaction the solvent was removed under reduced pressure to yield a residue. This crude product was directly used for the next step without further purifications.

General procedure for the reduction of γ-butyrolactone carboxylic acid

To a stirring solution of γ-butyrolactone carboxylic acid (1.0 equiv.) in THF (5.0 mL) was added $BH_3{\cdot}SMe_2$ (1.2 equiv.) drop-wise at room temperature and stirring was continued for another 6 h.[28] After the completion of the reaction the solvent was removed under reduced pressure to yield a residue which was purified by silica gel column chromatography using a gradient solvent system of 3–6% methanol in dichloromethane to yield γ-hydroxymethyl-γ-butyrolactone.

General procedure for the trityl protection of γ-hydroxymethyl-γ-butyrolactone

To a stirring solution of TrCl (1.1 equiv.) and triethylamine (1.2 equiv.) in dry dichloromethane, γ-hydroxymethyl-γ-butyrolactone (1.0 equiv.) in dry dichloromethane was added. The resulting mixture was stirred at room temperature for 12 h.[28] After completion of the reaction, the solvent was removed under reduced pressure to yield a residue. The residue was dissolved in dichloromethane (20 mL) and washed with a saturated solution of $NaHCO_3$. The organic layer was dried over anhydrous Na_2SO_4 and concentrated under reduced pressure. The residue was purified by silica gel column chromatography and a gradient solvent system of 20–30% ethyl acetate to hexane to give target compound.

General procedure for the aldol reaction

To a stirring solution of CuCN (1.0 equiv.) and LiCl (2.0 equiv.) in dry THF was added protected γ-hydroxymethyl-γ-butyrolactone (1.0 equiv.) under a N_2 atmosphere and the reaction mixture was stirred for 5 min at −78 °C, then *n*-BuLi (1.5 equiv., 1.5 M solution in THF) was added. Stirring was continued for 10 min at −78 °C and then aldehyde (1.5 equiv.) in dry THF was added drop-wise.[41] After completion of the reaction, the reaction was quenched with methanol/water and the solvent was removed under reduced pressure. The residue was dissolved in ethyl acetate and washed with saturated $NaHCO_3$ followed by brine solution. The organic layer was dried over anhydrous Na_2SO_4 and concentrated under reduced pressure. Column chromatography with silica gel and a gradient solvent system of ethyl acetate to hexane yielded the target protected alcohol.

General procedure for the preparation of esters

Carboxylic acid (1.1 equiv.), dicyclohexylcarbodiimide (1.1 equiv.) and *N*,*N*-dimethylaminopyridine (0.1 equiv.) were added to a stirring solution of the protected alcohol (1.0 equiv.) in anhydrous dichloromethane (5 mL) under a N_2 atmosphere.[34] Stirring was continued for 12 h at room temperature. After completion of the reaction, the reaction mixture was filtered and washed with dichloromethane. The filtrate was concentrated under reduced pressure and column chromatography was performed with silica gel and a gradient solvent system of 2–5% ethyl acetate to hexane.

General procedure for the removal of trityl-group

To a stirring solution of trityl-protected compound (1.0 equiv.) in dichloromethane (5.0 mL) was added TFA (2.0 equiv.) at room temperature and stirring was continued for 1 h.[28] After completion of the reaction, the solvent was removed under reduced pressure to yield a residue. The residue was dissolved in EtOAc (20 mL) and washed with a saturated solution of sodium bicarbonate. The organic layer was dried over anhydrous Na_2SO_4 and concentrated under reduced pressure. The residue was purified by silica gel column chromatography using 7–10% ethyl acetate to hexane to yield the target compound.

Aggregation studies

The aggregation behaviours of the compounds in aqueous solution were examined by fluorescence measurements at room temperature, using a Fluoromax-4 spectrofluorometer. The fluorescence properties of pyrene were monitored to measure the critical aggregation concentrations (CAC) of the compounds.[35,42] The stock solutions of compounds were freshly prepared by first dissolving them in spectroscopic-grade dimethylsulfoxide (DMSO) and then diluted with water. The amount of DMSO was kept less than 1% (by volume) for each set of experiments and had no effect on any experimental results. For fluorescence measurements, a saturated ethanolic solution of pyrene (2 μM) and varying concentrations of ligands were incubated in water at room temperature. Pyrene was excited at 335 nm, and emission spectra were recorded from 345 to 550 nm. Pyrene produces five intense fluorescence peaks, but only I_1 (373 nm) and I_3 (383 nm) were considered for measurements of CAC values.

Interfacial behaviour measurement by Langmuir trough techniques

The air–water interfacial behaviours of the amphiphilic compounds were investigated using the Langmuir trough technique (NIMA technology Ltd) according to the Wilhelmy plate method.[30,36] Stock solutions of the compounds were prepared in a chloroform/methanol mixture [4 : 1 (v/v)]. The sub-phase consisted of Milli-Q water (Millipore, Bedford, MA) and had a resistance of 18.4 MΩ cm. Before each experiment the cleanliness of the sub-phase was verified by repeated compression without lipids. If the surface pressure changed by less than 0.2 mN m^{-1} then the surface was considered to be clean. Lipid solutions (5 μL of 0.5 mg mL^{-1} stock solution) were deposited onto the surface of the sub-phase. After the solvent had been allowed to evaporate for 10 min, the monolayer was compressed at a constant rate of 10 mm min^{-1}, and the surface pressure (π)–area (A) isotherm was continuously recorded. All experiments were conducted at room temperature (25 °C). The π–A isotherm was analysed by inbuilt software.

Measurement of the change in bilayer fluidity and hydration

To measure the change in membrane fluidity, anisotropy of DPH under liposomal environment was measured according to the reported procedure.[43] The fluorescence probe DPH was incorporated into the liposomes by adding the dye dissolved in THF (1 mM) to liposomes (PC/cholesterol/ligand (60/20/20)) up to a final concentration of 1.25 μM. After 30 min of incubation at room temperature DPH fluorescence anisotropy was measured at 430 nm (excitation 355 nm). The concentration of compounds was 2.9 μM. To measure the change of membrane hydration, dansyl-PE doped liposomes (PC/cholesterol/dansyl-PE (79/20/1)) were prepared separately with and without doping of membrane active HGL compounds at different concentrations (0–80 mol%) and the change in dansyl fluorescence signal was recorded.[32,33]

Extent of membrane localization

The extent of localization of the compounds at the liposome–water interface was compared by the NBD fluorescence quenching method using PC/ligand$_{16}$/NBD-PE liposomes (89/10/1) in 50 mM Tris buffer, pH 8.2, containing 150 mM NaCl, according to the reported procedure.[43] The NBD fluorescence quenching reaction was initiated by adding sodium dithionite solution (a stock solution of 0.6 M sodium dithionite in 50 mM Tris buffer, pH 11, and containing 150 mM NaCl, was used to obtain a final concentration of 1 mM). The change in NBD fluorescence emission intensity at 530 nm (λ_{ex} = 469 nm) was recorded for 3 min at room temperature.

Protein purification

The C1b subdomain of PKCδ and PKCθ isoforms were expressed in *E. coli* cells and purified by using methods similar to those reported earlier.[35,43]

Fluorescence-based protein binding analysis

To compute the binding parameters under a membrane-free system, ligand-induced Trp-fluorescence quenching measurements were performed on a Fluoromax-4 spectrofluorometer at room temperature.[34,35] The stock solutions of compounds were freshly prepared by first dissolving complexes in spectroscopic-grade DMSO and then diluted with buffer. The amount of DMSO was kept less than 3% (by volume) for each set of experiments and had no effect on any experimental results. For fluorometric titration, protein (1 μM) and varying concentrations of compounds were incubated in a buffer solution (20 mM Tris, 150 mM NaCl, 50 μM $ZnSO_4$, pH 7.4) at room temperature. Protein was excited at 284 nm, and emission spectra were recorded from 300 to 550 nm. Proper background corrections were made to avoid the contribution of buffer and dilution effects. The resulting plot of Trp-fluorescence as a function of ligand concentration was subject to nonlinear least-squares best-fit analysis to calculate apparent dissociation constants for the monomeric ligands (K_D(ML)), using eqn (1), which describes binding to a single independent site.

$$(F_0 - F) = \Delta F_{max}\left(\frac{[x]}{[x] + K_D(\mathrm{ML})}\right) + C \qquad (1)$$

where F and F_0 represented the fluorescence intensity at 339 nm in the presence and the absence of ligand respectively. The ΔF_{max} represents the calculated maximal fluorescence change; $[x]$ represents the total monomeric ligand concentration.

Fluorescence anisotropy measurements were also performed on the same fluorimeter using reported method.[34,35] All anisotropy values of the proteins in the absence or presence of compounds are the mean values of three individual determinations. The degree (r)

of anisotropy in the tryptophan fluorescence of the proteins was calculated using eqn (2), at the peak of the protein fluorescence spectrum, where I_{VV} and I_{VH} are the fluorescence intensities of the emitted light polarized parallel and perpendicular to the excited light, respectively, and $G = I_{VH}/I_{HH}$ is the instrumental grating factor.

$$r = \frac{(I_{VV} - GI_{VH})}{(I_{VV} + 2GI_{VH})} \quad (2)$$

Protein-to-membrane Förster resonance energy transfer (FRET) based binding assay was used to measure the binding affinity and specificity of the selected compounds under the liposomal environment.[34,35] In this assay, membrane-bound C1 domain was displaced from liposomes by the addition of the DAG_8. The liposomes composed of PC/PE/PS/dPE (60/15/20/5) and PC/PE/PS/dPE/ligand (55/15/20/5/5) were used as control and for ligands, respectively. The stock solution of DAG_8 was titrated into the sample containing C1 domain (1 μM) and excess liposome (100 μM total lipid) in a buffer solution (20 mM Tris, 150 mM NaCl, 50 μM $ZnSO_4$, pH 7.4) at room temperature. The competitive displacement of protein from the membrane was quantitated using a protein-to-membrane FRET signal (λ_{ex} = 280 nm and λ_{em} = 505 nm). Control experiments were performed to measure the dilution effect under similar experimental conditions and the increasing background emission arising from direct dPE excitation. Protein-to-membrane FRET signal values as a function of DAG_8 concentration were subjected to nonlinear least-squares-fit analysis using eqn (3) to calculate apparent equilibrium inhibition constants ($K_I(DAG_8)_{app}$) for DAG_8. Where, [x] represents the total DAG_8 concentration and ΔF_{max} represents the calculated maximal fluorescence change.

$$F = \Delta F_{max}\left(1 - \frac{[x]}{[x] + K_I(DAG_8)_{app}}\right) + C \quad (3)$$

The equilibrium dissociation constant (K_D(L)) for the binding of the C1 domains to the ligand-associated liposomes was calculated from eqn (4), using K_D(ML) and $K_I(DAG_8)_{app}$ values,[34,35] where $[L]_{free}$ is the free ligand concentration (2.63 ± 0.04 μM). During calculations the ligand concentrations in the liposome interior were ignored because of their inaccessibility for the protein. Thus, the protein accesses about half of lipids in the liposomes. The ligand concentration was used in excess relative to the protein. The free ligand concentration was calculated by assuming that most of the protein would bind to the liposome and an equimolar amount of ligand can be subtracted from the accessible ligand.

$$K_I(DAG_8)_{app} = K_D(ML)\left(1 + \frac{[L]_{free}}{K_D(L)}\right) \quad (4)$$

We also measured direct liposome binding of PKC C1b subdomains using a Trp-fluorescence quenching method. The protein (0.25 μM) was added to PC/PE/PS/ligand$_{16}$ (55/20/20/5) liposomes prepared by an extrusion method. Fluorescence intensity values were plotted against the liposomes containing ligand concentrations to generate the binding isotherms using eqn (1).

Molecular modelling

Molecular docking analysis was performed using the crystal structure of PKCδ–C1b (Protein Data Bank code: 1PTR) subdomain.[37] The generation of energy minimized three-dimensional structures of ligands and ligand–protein docking was performed using methods similar to those described earlier. Briefly, the energy-minimized three-dimensional structure of ligands was prepared by using the GlycoBioChem PRODRG2 Server.[44] Ligand–protein docking was performed using the Molegro Virtual Docker software, Version 4.3.0 (Molegro ApS, Aarhus, Denmark).[45] The binding site was automatically detected by the docking software and restricted within spheres with a radius of 15 Å. During docking analysis the following parameters were kept unchanged: number of runs 10, population size 50, crossover rate 0.9, scaling factor 0.5, maximum iteration 5000 and grid resolution 0.30. The docking results were examined on the basis of moledock and re-rank scores. The docking poses were exported and re-examined with PyMOL visualization software.

PKC activity analysis

The PKC enzyme activity was measured using a PepTag non-radioactive protein kinase assay kit in the presence of DAG_{16} and potent compounds with a modified assay protocol. The assay was stopped after 30 min by incubating the sample vials at 95 °C for 10 min and then 2 μL of 80% glycerol was added to the samples. Agarose gel (0.8%) electrophoresis was run at 110 V for 20 min and the gel image was captured under UV light. The phosphorylated fluorescent peptide bands were excised from agarose gel, and PKC activity was quantitatively estimated by fluorescence spectral analysis (λ_{ex} = 540 nm).

	Reagents for the assay	Control (μL)	Reactions (μL)
1	PepTag PKC reaction 5× buffer	5	5
2	PepTag C1 peptide (0.4 μg μL^{-1})	5	5
3	PKC activator 5× solution	0	5
4	Compounds (DAG/**1a**/**2a**/**3a**; 80 μM)	0	2.5
5	Peptide protection solution	1	1
6	Protein kinase C (2.5 μg mL^{-1} in PKC dilution buffer)	4	4
7	Deionized water for final reaction volume of 25 μl	5	2.5

Acknowledgements

The authors acknowledge their sincere gratitude to the Department of Chemistry, Centre for the Environment, Central Instrumentation Facility, Indian Institute of Technology Guwahati,

India. The authors are also thankful to the CSIR (02(0090)/12/EMR-II) Govt. of India for financial support.

Notes and references

1 M. J. Wakelam, *Biochim. Biophys. Acta*, 1998, **1436**, 117–126.
2 S. G. Rhee, *Annu. Rev. Biochem.*, 2001, **70**, 281–312.
3 G. Manning, D. B. Whyte, R. Martinez, T. Hunter and S. Sudarsanam, *Science*, 2002, **298**, 1912–1934.
4 E. M. Griner and M. G. Kazanietz, *Nat. Rev. Cancer*, 2007, **7**, 281–294.
5 A. C. Newton and L. M. Keranen, *Biochemistry*, 1994, **33**, 6651–6658.
6 Y. Nishizuka, *Science*, 1992, **258**, 607–614.
7 F. Battaini and D. Mochly-Rosen, *Pharmacol. Res.*, 2007, **55**, 461–466.
8 J. Li, B. P. Ziemba, J. J. Falke and G. A. Voth, *J. Am. Chem. Soc.*, 2014, **136**, 11757–11766.
9 A. C. Newton, *Chem. Rev.*, 2001, **101**, 2353–2364.
10 G. Boije Af Gennas, V. Talman, J. Yli-Kauhaluoma, R. K. Tuominen and E. Ekokoski, *Curr. Top. Med. Chem.*, 2011, **11**, 1370–1392.
11 C. E. Antal, A. M. Hudson, E. Kang, C. Zanca, C. Wirth, N. L. Stephenson, E. W. Trotter, L. L. Gallegos, C. J. Miller, F. B. Furnari, T. Hunter, J. Brognard and A. C. Newton, *Cell*, 2015, **160**, 489–502.
12 G. Boije af Gennas, V. Talman, O. Aitio, E. Ekokoski, M. Finel, R. K. Tuominen and J. Yli-Kauhaluoma, *J. Med. Chem.*, 2009, **52**, 3969–3981.
13 R. V. Stahelin, *J. Lipid Res.*, 2009, **50**(suppl), S299–S304.
14 H. J. Mackay and C. J. Twelves, *Nat. Rev. Cancer*, 2007, **7**, 554–562.
15 A. J. Cameron, K. J. Procyk, M. Leitges and P. J. Parker, *Int. J. Cancer*, 2008, **123**, 769–779.
16 R. Zeidman, B. Lofgren, S. Pahlman and C. Larsson, *J. Cell Biol.*, 1999, **145**, 713–726.
17 D. L. Alkon, M. K. Sun and T. J. Nelson, *Trends Pharmacol. Sci.*, 2007, **28**, 51–60.
18 J. P. Arcoleo and I. B. Weinstein, *Carcinogenesis*, 1985, **6**, 213–217.
19 N. Kedei, D. J. Lundberg, A. Toth, P. Welburn, S. H. Garfield and P. M. Blumberg, *Cancer Res.*, 2004, **64**, 3243–3255.
20 J. Kortmansky and G. K. Schwartz, *Cancer Invest.*, 2003, **21**, 924–936.
21 J. Koivunen, V. Aaltonen and J. Peltonen, *Cancer Lett.*, 2006, **235**, 1–10.
22 J. H. Kang, Y. Kim, S. H. Won, S. K. Park, C. W. Lee, H. M. Kim, N. E. Lewin, N. A. Perry, L. V. Pearce, D. J. Lundberg, R. J. Surawski, P. M. Blumberg and J. Lee, *Bioorg. Med. Chem. Lett.*, 2010, **20**, 1008–1012.
23 V. E. Marquez and P. M. Blumberg, *Acc. Chem. Res.*, 2003, **36**, 434–443.
24 V. Talman, R. K. Tuominen, G. B. af Gennas, J. Yli-Kauhaluoma and E. Ekokoski, *PLoS One*, 2011, **6**, e20053.
25 O. Raifman, S. Kolusheva, M. J. Comin, N. Kedei, N. E. Lewin, P. M. Blumberg, V. E. Marquez and R. Jelinek, *FEBS J.*, 2010, **277**, 233–243.
26 P. M. Blumberg, N. Kedei, N. E. Lewin, D. Yang, G. Czifra, Y. Pu, M. L. Peach and V. E. Marquez, *Curr. Drug Targets*, 2008, **9**, 641–652.
27 S. Benzaria, B. Bienfait, K. Nacro, S. M. Wang, N. E. Lewin, M. Beheshti, P. M. Blumberg and V. E. Marquez, *Bioorg. Med. Chem. Lett.*, 1998, **8**, 3403–3408.
28 C. Pathirana, R. Dwight, P. R. Jensen, W. Fenical, A. Delgado, L. S. Brinen and J. Clardy, *Tetrahedron Lett.*, 1991, **32**, 7001–7004.
29 R. Borah, D. Talukdar, S. Gorai, D. Bain and D. Manna, *RSC Adv.*, 2014, **4**, 25520–25531.
30 M. Hubert, B. J. Compton, C. M. Hayman, D. S. Larsen, G. F. Painter, T. Rades and S. Hook, *Mol. Pharmaceutics*, 2013, **10**, 1928–1939.
31 M. A. Bos, B. Vennat, M. T. Meunier, M. P. Pouget, A. Pourrat and J. Fialip, *Biol. Pharm. Bull.*, 1996, **19**, 146–148.
32 L. W. Runnels, J. Jenco, A. Morris and S. Scarlata, *Biochemistry*, 1996, **35**, 16824–16832.
33 C. Ho, S. J. Slater and C. D. Stubbs, *Biochemistry*, 1995, **34**, 6188–6195.
34 N. Mamidi, R. Borah, N. Sinha, C. Jana and D. Manna, *J. Phys. Chem. B*, 2012, **116**, 10684–10692.
35 D. Talukdar, S. Panda, R. Borah and D. Manna, *J. Phys. Chem. B*, 2014, **118**, 7541–7553.
36 N. Mamidi, S. Gorai, B. Ravi and D. Manna, *RSC Adv.*, 2014, **4**, 21971–21978.
37 G. G. Zhang, M. G. Kazanietz, P. M. Blumberg and J. H. Hurley, *Cell*, 1995, **81**, 917–924.
38 D. Duan, D. M. Sigano, J. A. Kelley, C. C. Lai, N. E. Lewin, N. Kedei, M. L. Peach, J. Lee, T. P. Abeyweera, S. A. Rotenberg, H. Kim, Y. H. Kim, S. El Kazzouli, J. U. Chung, H. A. Young, M. R. Young, A. Baker, N. H. Colburn, A. Haimovitz-Friedman, J. P. Truman, D. A. Parrish, J. R. Deschamps, N. A. Perry, R. J. Surawski, P. M. Blumberg and V. E. Marquez, *J. Med. Chem.*, 2008, **51**, 5198–5220.
39 S. K. Sukumaran and N. V. Prasadarao, *J. Biol. Chem.*, 2002, **277**, 12253–12262.
40 V. A. Verriere, D. Hynes, S. Faherty, J. Devaney, J. Bousquet, B. J. Harvey and V. Urbach, *J. Biol. Chem.*, 2005, **280**, 35807–35814.
41 O. Z. Pereira and T. H. Chan, *Tetrahedron Lett.*, 1995, **36**, 8749–8752.
42 Q. Zhang, Z. Gao, F. Xu, S. Tai, X. Liu, S. Mo and F. Niu, *Langmuir*, 2012, **28**, 11979–11987.
43 N. Mamidi, S. Panda, R. Borah and D. Manna, *Mol. BioSyst.*, 2014, **10**, 3002–3013.
44 A. W. Schuttelkopf and D. M. van Aalten, *Acta Crystallogr., Sect. D: Biol. Crystallogr.*, 2004, **60**, 1355–1363.
45 R. Thomsen and M. H. Christensen, *J. Med. Chem.*, 2006, **49**, 3315–3321.